How to Model the Conformational Behaviour of Saturated Diphosphane Chelate Cycles: The Conformational Rearrangement Processes of [{κ-$PAr_2CH_2CH(OH)CH_2$-κ-PAr'_2}Rh-(η^4-COD)]$^+$

Volker Schulz,[a] Axel Frick,[a] and Gottfried Huttner*[a]

In memoriam Dr. Laszlo Zsolnai[†]

Keywords: Rhodium / Phosphane ligands / Chelates / Molecular modelling / Conformation analysis

Eleven solid state structures of eight compounds **1**–**8** of the type [{κ-$PAr_2CH_2CH(OH)CH_2$-κ-PAr'_2}Rh-(η^4-COD)]$^+PF_6^-$ are used as a basis for deriving a force field model for this class of compound by Genetic Algorithms. By a complete search in the conformational space of [{κ-$PMes_2CH_2$-$CH(OH)CH_2$-κ-PPh_2}Rh-(η^4-COD)]$^+PF_6^-$ (**1**) it is shown that the model is not only capable of reproducing the structures but as well capable to predict the stability of individual conformers and the conformational reaction pathways in full agreement with experimental observations. The model predicts that the λ twist conformation is the most stable conformation of **1**. The δ twist conformation is calculated 3.1 kJ·mol^{-1} above this minimum. The experimental value is 3.4 kJ·mol^{-1}. The model predicts that there are two mechanistic pathways for the λ ⇄ δ isomerization process. Both of them are characterised by a strictly coupled rotation of the mesityl groups of the $PMes_2$ entity of **1**. These two pathways differ only in the sense of this rotation. The activation enthalpy for the λ ⇄ δ isomerization process as a whole is calculated as $\Delta H^{\#}$ = 69.1 kJ·mol^{-1}. The experimental value is $\Delta H^{\#}$ = 64.4 kJ·mol^{-1}. It is concluded therefore that the novel type of approach as described leads to models of very high predictive power.

Introduction

Molecular mechanics has been established to be a highly efficient tool in understanding the conformational manifold of small organic molecules.[1,2] In coordination chemistry these methods should work as well, once the force field parameters describing the metal ligand interactions would be known. The fact, however, that there are many different metals along the periodic table and that all these metals may engage with the ligands in different geometries makes the molecular mechanics approach in general a cumbersome one.[3−5] Nevertheless different types of general force fields have been described which are in fact able to overcome many of these difficulties and are able to predict conformations of inorganic and organometallic compounds.[6,7] Such force fields are, however, limited in the accuracy with which they predict the energy differences between individual conformers. If, on the other hand, conformational pathways are at the focus of a molecular mechanics analysis and if the calculated energy differences are small and are to be compared to experimentally determined reaction enthalpies these generalised force fields do not reproduce energies to the desired and necessary accuracy.[8]

As an alternative to generalised force fields specific force fields may be developed for a specific class of compounds.[3−5] It may be hoped that such specific force fields might be able to reproduce not only the geometry but as well the relative energy of the conformational manifold in agreement with experimental data.[9,10] Such force fields, if developed in the traditional way, have been shown to correctly reproduce conformations while the energies of these conformations are still generally not reliable enough to compare small energy differences to experimental data. It is common practice to adjust force field parameters of a specific class of compound by hand such that a known structure is correctly reproduced and to optimise the parameters by trial-and-error on the basis of a few experimentally determined structures of the specific class of compounds analysed. Parameters thus obtained may be taken as such or may be used as a starting point for further optimisation. The optimisation procedures used in this case are local ones, i.e. they will lead to a locally optimised set of parameters which need not necessarily be the optimal solution of the global problem.

With this in mind optimisation procedures have been developed which − starting from a randomly selected point in parameter space − allow for a global search of the optimal

[a] Anorganisch-Chemisches Institut der Universität Heidelberg, Im Neuenheimer Feld 270, 69120, Germany
Fax: (internat.) + 49 (0)6221/545707
E-mail: g.huttner@indi.aci.uni-heidelberg.de
[†] August 18, 1947−April 26, 1998

set of parameters.[11−16] While optimisation procedures which will solve this type of problem with certainty within an finite amount of time are not available, optimisation by Genetic Algorithms has been found to be an efficient way around this problem in many situations.[17−19] It has in fact been shown that force fields derived by this strategy are well suited to predict structures as well as energy differences in agreement with experimental observations.[11−16] This kind of approach has been applied to analyse and predict the conformational properties of *tripod*-$Mo(CO)_3$ compounds [*tripod* = $RCH_2C(CH_2PR'_2)(CH_2PR''_2)(CH_2PR'''_2)$]. By this method it was possible to predict NOE-distances of compounds such as $CH_3C[CH_2P(R')(CH_2Ph)]_3Mo(CO)_3$ (R′ = Ph, 3,5-Xylyl) to within an rms of less than 0.3 Å with respect to the experimental values.[15] The same type of approach was used to predict the activation barriers of the conformational isomerisation of compounds $[CH_3C\{CH_2P(Ph)_2\}_{3-n}\{CH_2P(o\text{-Tol})_2\}_n]Mo(CO)_3$ (n = 1−3) to within less than 5 kJ·mol^{-1}.[16]

The quality of these results suggests that it might be worthwhile to apply a similar strategy to more complicated problems. 'More complicated' in this context means that there is a larger number of torsional degrees of freedom which cover a wide spread of torsion angles. In the *tripod* metal compounds analysed by now the chelate scaffolding of the bicyclo[2.2.0.]octane type is such that the individual six-membered chelate cycles are forced to adopt boat or twist conformations with any chair conformation excluded by the rigidity of the framework. In this sense the conformations of compounds of the type $[\{\kappa\text{-}PAr_2CH_2CH(OH)CH_2\text{-}\kappa\text{-}PAr'_2\}Rh\text{-}(\eta^4\text{-}COD)]^+PF_6^-$ are more complicated since the six-membered chelate cycles − which are not a part of a chelate cage − can adopt boat, twist or chair conformations.

Compounds of this type have been shown to be efficient precatalysts in the enantioselective hydrogenation of olefins.[20] The solid state structures of eleven members of this family of compounds are known[20] which are well suited as a basis to derive appropriate force field parameters by Genetic Algorithms. In addition, the solution structures of four of these compounds are known as well as the activation barriers for different types of conformational rearrangements.[8] With all these data given this class of compounds presents an ideal object for evaluating the power of the modelling approach as sketched above. In addition the problem is of some chemical interest since the conformational properties of six-membered diphosphane chelate cycles have not been analysed in detail, while, of course, it is just these properties which will control the stereochemical result of reactions mediated by chelate compounds containing these cycles.

Results and Discussion

The paper deals with the following problems:

"Definition of the Force Field"

− How to describe the forces which imply contributions by the metal?

"Optimisation of Force Field Parameters"

− How to optimise this description by Genetic Algorithms?

"Grid Search Analysis of 1−3"

− How to do a complete scan of the conformational hypersurface?

"Energy − Reaction Pathway"

− How to analyse conformational pathways and how to derive activation energies for these pathways?

"Force Field Model and Experimental Reality − Comparison of Results and Conclusion"

− How do the calculated results compare to the experimental ones?

The compounds **1**−**8** on which the analysis of these questions is based are shown in Figure 1. For some compounds δ and λ twist forms where found in one and the same crystal. In these cases the two crystallographically independent conformations have been dealt with as independent individual molecules.

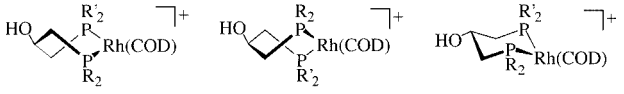

Compound	Structure	PR_2	PR'_2	X-ray		Chirality
1	**1a**	$PMes_2$	PPh_2	twist	δ	(S)
1	**1b**	$PMes_2$	PPh_2	twist	λ	(S)
2	**2a**	PPh_2	$P(o\text{-Tol})_2$	chair	OH-*eq*	(R)
3	**3a**	DBP	$P(o\text{-Tol})_2$	chair	OH-*eq*	(S)
4	**4a**	$PMes_2$	PEt_2	twist	δ	(S,R)
5	**5a**	$PMes_2$	$P(2\text{-MeOPh})_2$	twist	λ	(R)
5	**5b**	$PMes_2$	$P(2\text{-MeOPh})_2$	twist	δ	(R)
6	**6a**	$P(2\text{-MeOPh})_2$	PPh_2	twist	λ	(S)
6	**6b**	$P(2\text{-MeOPh})_2$	PPh_2	twist	δ	(S)
7	**7a**	$P(o\text{-Tol})_2$	PEt_2	chair	OH-*eq*	(S,R)
8	**8a**	PPh_2	PPh_2	chair	OH-*eq*	

Figure 1. Compounds **1**−**8**; the sequence in which the compounds are labelled is such that compounds **1**−**3** are the ones which are extensively analysed in this paper. For compounds **1**, **2**, **4**, **5** quantitative solution structures are available.[8] Qualitative NMR spectroscopic data for dynamic processes are available for **6**, **7**.[20] The numbering scheme follows this hierarchy.

Definition of the Force Field

Parameters describing interactions within the organic parts of the molecules were taken from the standard MM2* force field.[1,21,22] Parameters describing C−P−C angles

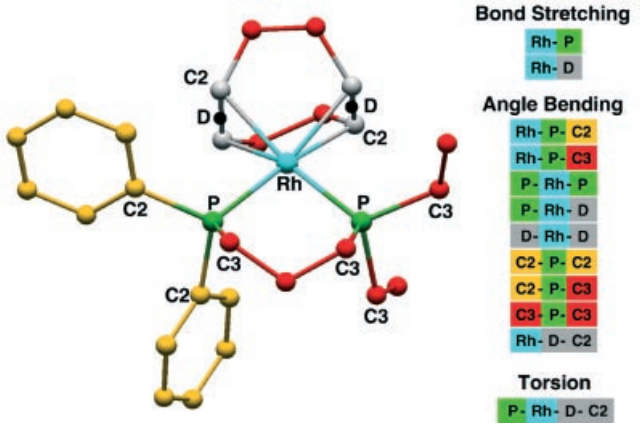

Figure 2. Illustration of the force field parameters which were refined; the colours refer to the individual atom types (C2: sp^2-carbon; C3: sp^3-carbon). The label D designates a dummy atom placed at the centre of a double bond of the COD ligand. Only the parameters which are listed in Figure 2 were allowed to refine.

(Figure 2) were defined as usual − they were however refined (see below). All parameters involving the rhodium atom were refined. Conventional descriptions were used to describe distances, angles and torsion angles (see Exp. Sect.).

Parameters involving parts of the COD coligand and the metal atom where defined as follows: dummy atoms were defined at the centre of each coordinated double bond (Figure 3). The distances between the dummy atoms and the rhodium centre (r_d, Figure 3) as well as the angles D−Rh−D (β, Figure 3) and D−Rh−P (γ, Figure 3) were described by conventional functionals (see Exp. Sect.). The angles enclosed by the rhodium centre, the dummy atoms and any of the two carbon atoms of the double bond adjacent to the dummy atom Rh−D−C2 (α, Figures 2 and 3) were as well modelled by the standard functional for valence angles (see Exp. Sect.). To define the rotational position of the π-ligands with respect to the rest of the molecule the rotation of the double bond around the axis Rh−D was defined by the torsion angle around this axis. The reference axis was defined as a Rh−P vector. Of the two Rh−P vectors the one was chosen whichever had the smaller D−Rh−P angle. The torsion angle (see Exp. Sect.) was defined with respect to one of the vectors D−C2 (Figures 2 and 3). The energy function for this angle (τ, Figure 3) was

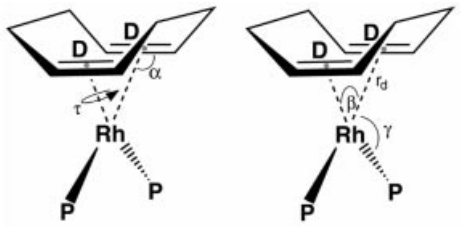

Figure 3. Definition of π bonds within the force field approach. Dummy atoms at the centre of the coordinated double bonds were used to define the parameters r_d, α, β, γ, and τ. The forces acting on the dummy atoms were distributed to the two carbon atoms of the respective double bonds. Half of the force acting upon D was assigned to each of these atoms.

chosen as $E(\tau) = k_{t2}\cdot[1 - \cos(2\tau)]$. τ values of ±90° correspond to an orientation of the double bond vertical to the coordination plane of the rhodium atom. These positions correspond to minima in the torsional potential function $E(\tau) = k_{t2}\cdot[1 - \cos(2\tau)]$ where the force constant k_{t2} has hence to be negative. τ values of ±90° correspond to the situation sketched in Figure 3 which is a minimum situation with cos(2τ) being −1. The forces on the dummy atoms have to be transferred to the carbon atoms of the double bonds to which they refer. The force field thus defined was incorporated in the body of the force field program YAMMP[23] (see Exp. Sect.).

This type of approach is similar to the one be taken by B. Bosnich and C. R. Landis et. al. for the force field description of coordinated Cp ligands.[24,25] Similar methods have been developed by van Gunsteren[26] for the force field description of proteins and by C. R. Landis et. al. for descriptions of different types of π-ligands.[27]

Optimisation of Force Field Parameters

In order to describe conformational behaviour by force field methods an algorithmic machinery is needed which correctly models the experimentally determined behaviour. Such a machinery has to be built up with appropriate functions and parameters. Once the functions are defined it is the parameters which have to be tuned. Tuning means to adapt the parameters such that the observed conformational properties of the molecule are correctly reproduced by the machinery. The conformational property chosen in most cases is the 'structure' of the molecule. Structures, however, are in general taken from crystallographic studies; this means that the molecule is embedded in a crystal and subject to external forces acting upon it from the neighbouring molecules. If force field parameters are fitted to reproduce such structures it is the solid state structures which they reproduce. Only if it is evident that these structures, even though determined in the solid state, are almost completely due to the inner molecular potential with vanishing contributions from the external forces, this approach will lead to a force field which models the inner molecular potential. If a large number of a family of crystal structures is known the question of whether these structures are by and large uninfluenced by crystal forces can be addressed by statistical analysis. In the first report on the use of Genetic Algorithms in the refinement of force field parameters which dealt with modelling the behaviour of *tripod*-$Mo(CO_3)$ compounds[14] statistical analysis by a variety of methods including Neural Network analysis had shown that these premises are met in this case.[11] Refinement of the force field parameters on the basis of solid state structures has been highly successful in this case.[14] In the present case there are too few individual structures available for a meaningful statistical test. A practical approach in this case is then to assume that the crystal structures are due to the inner molecular potentials, to refine the force field parameters on this basis and possibly to remove outliers if there are any. It is assumed in this case that structures which are less well reproduced than the average are influenced by

crystal forces acting on the molecules in the crystal lattice. This approach is taken in this paper.

Genetic Algorithms were applied to tune the force field parameters such that twelve crystallographically determined structures of the eight compounds (Figure 1) were reproduced to the best possible extent. A short explanation of how Genetic Algorithms work, may help to appreciate that the methodology is very simple indeed. The first thing to do is to make a guess for the numerical range which the individual parameters may possibly adopt. To give an example: it is known that the valence force constants can adopt values up to a maximum of 20 mdyn·Å^{-1} and, of course, that such force constants have to be greater than zero. In this case setting the range for this type of constant to $0 \leq k \leq 20$ covers all possible values. If it is known that the specific force constant k refers to a weak bond this range might be much smaller of course. Once the numerical range is determined it is divided in $2^{(n-1)}$ equally spaced intervals. The position of each specific interval may then be clearly defined by a binary number in the range $0 \leq 2^{n-1}$. The binary number may thus be taken as a representation of a numerical interval within the range allotted to the parameter. It may be decoded into the numerical value of this parameter with the resolution depending on the size of the interval.[28]

To start the optimisation process binary representations of the values of the individual parameters are generated stochastically. The binary representations of the individual parameters are combined in one binary string where the positions on the string clearly indicate to which parameter each part of the string belongs. A whole set of such parameter strings is generated; in the Genetic Algorithm idiom it is called a population (Figure 4). Each parameter string is decoded to produce the numerical values of the individual parameters. The parameters are fed into the force field program and the experimentally determined structures are subject to refinement. The quality of a given set of parameters is deduced by their capability to produce a set of refined structures in close agreement with the experimentally determined conformations. By some formalism this quality is expressed as a number. In the example given (Figure 4) a small number is meant to indicate a high quality and a large one to correspond to a low quality parameter set. The numerical values by which the sets are ranked are called the fitness values in the Genetic Algorithm idiom. For each individual within a given population this fitness is evaluated on the basis of all observations. With the problem at hand this means that for a given set of force field parameters each of the structures in the data base has to be optimised. This has to be done for all individuals of a population within each generation over and over again and thus is the really time consuming part within optimisations based on Genetic Algorithms. Optimisation itself is achieved by creating a next generation of parameter sets from the forgoing one such that the population of this next generation has a high probability to contain bit strings or parts of bit strings which had already been shown to produce high fitness values in the foregoing generation. This is achieved by making fit individuals produce offspring with higher probability than the less fit ones. Offspring is generated by exchanging parts of bit strings between the parents (Figure 4) that is by crossover. The idea behind this is that pieces of information (bit strings) which have already been found to be well adapted to solve the problem will accumulate from generation

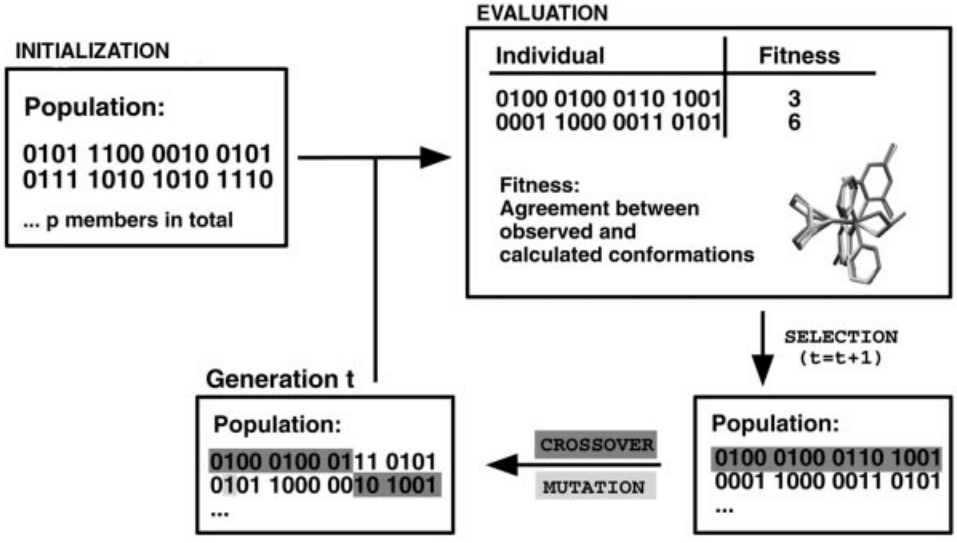

Figure 4. Refinement of the force field parameters by Genetic Algorithms. The parameters which are to be refined are encoded as binary strings. The sections within these strings refer to individual parameters. The values of these parameters are represented by the binary numbers within these sections. The first generation of such strings is generated at random. Each of these parameter strings is evaluated with respect to the quality with which it is capable of reproducing the structures of all compounds in the data basis by molecular mechanic calculations. The parameters which have a high 'fitness value' are preferentially selected to produce offspring by crossover and mutation. The next generation thus produced is subject to the same procedure of evaluation and offspring production. Iteration of this process leads to optimised parameters.

to generation such that the populations as a whole and their individual members will be more and more adapted to the problem from generation to generation. In order to avoid that the selection procedure leads to a suboptimal solution mutations are induced once in a while by inverting randomly selected bits (Figure 4).[29,30]

The optimisation by Genetic Algorithm (GA-optimisation) is generally an efficient optimisation strategy converging to optimal solutions also in those cases where traditional optimisation procedures fail.[31−33] A specific advantage of the underlined algorithmic scheme is that the time consuming step (evaluation of the fitness) may be performed independently on different processors, i.e. the algorithm is naturally parallel. With the problem at hand reasonable computing times can only be achieved if optimisations are performed on a parallel computer.

With the problem at hand GA-optimisation led to force field parameters, which when fed into the molecular mechanics program, were able to reproduce the observed structures. It was found that the agreement between calculated and observed structures was quite good for eleven members of this set (**1**−**8**) while one structure {**2b**: [{κ-PPh_2CH_2CH-$(OH)CH_2$-κ-P(*o*-Tol)$_2$}Rh-(η^4-COD)]$^+PF_6^-$} was less well reproduced. Analysis of the crystal structure indicated that the observed conformation might be biased by crystal forces and structure **2b** was therefor excluded from the data basis.[34] Refinement based on the optimisation of the eleven remaining structures led to satisfactory agreement for all the members of the set (Table 1 and Figure 5).

Table 1. RMS deviations of structures **1a**−**8a**

Structure[a]	RMS_{mm2_rms} [Å]	RMS_{mm2_int} [Å]
1a	0.343	0.368
1b	0.212	0.256
2a	0.384	0.441
3a	0.238	0.267
4a	0.357	0.249
5a	0.253	0.242
5b	0.286	0.284
6a	0.191	0.190
6b	0.195	0.187
7a	0.136	0.165
8a	0.196	0.284
average	0.254	0.267

[a] The column with the suffix mm2_rms was obtained on the basis of parameters calculated by using the RMS deviations between observed and calculated atom positions as the criteria to evaluate the fitness. The column labelled mm2_int refers to a parameter set which was obtained by basing the evaluation of fitness on the agreement between calculated and experimental values of a set of selected internal coordinates (optimised distances, angles, and torsion angles).

Expressed as the RMS deviation between observed and calculated atom positions the agreement is between 0.14 and 0.38 Å. Table 1 refers to two different procedures used for the evaluation of fitness during Genetic Algorithm refinement. The column with the suffix mm2_rms was obtained on the basis of parameters calculated by using the RMS deviations between observed and calculated atom positions as the criteria to evaluate the fitness. The column labelled mm2_int refers to a parameter set which was obtained by basing the evaluation of fitness on the agreement between calculated and experimental values of a set of selected internal coordinates (optimised distances, angles, and torsion angles). Independent of the criteria on which the evaluation of fitness was based, the refined parameter sets were able to reproduce the structures quite well. Figure 5 shows an overlay of observed and calculated conformations for an unbiased (cf. Table 1) selection of compounds.

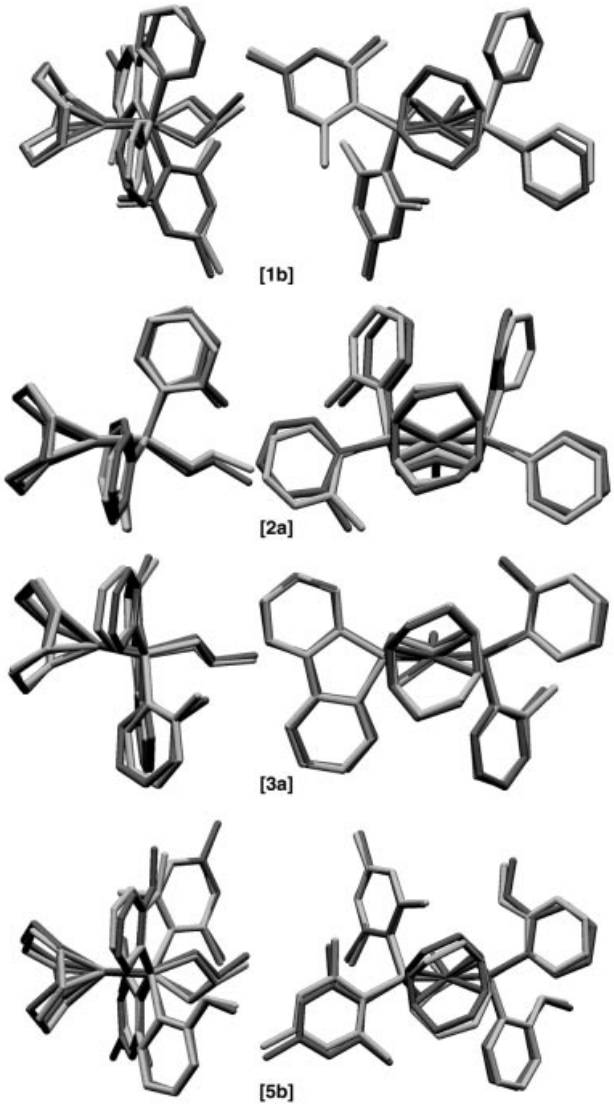

Figure 5. Illustration of the quality of agreement between calculated and observed conformations. From the compounds shown **2a** is the one with the lowest quality of reproduction (Table 1). The other compounds shown are of average quality.

Numerical values of force constants optimised by this approach have their meaning only as a whole: due to the interdependence of the internal coordinates which are used to describe the mechanical model within a force field program there is in general not just one optimal solution to the optimisation but there may be families of optimal solutions with quite different numerical values for the individual force

constants. When fed into a molecular modelling program as a whole these numerically different solutions will equally well reproduce the structures.

Table 2 shows the quality of agreement with respect to internal coordinates. The columns labelled average in Table 2 show that the average of the values for individual types of distances, angles and torsion angles taken over all structures are well reproduced by the two parameter sets. The force field mm2_int derived by minimising the discrepancy between observed and calculated values of internal coordinates is found to reproduce such internal coordinates (distances, angles, and torsion angles) somewhat better than the mm2_rms which minimises the discrepancy between atom positions (Table 2). The columns labelled rmsd represent the RMS deviation between calculated and observed values in each case. These deviations must be larger than the deviations between corresponding average values (Table 2) since in calculating the average positive and negative deviations may cancel each other while in calculating the RMS deviation (rmsd) they are accumulating independent of sign. From the numbers given in Table 2 it is seen for set mm2_rms that some valence angles are systematically too large or too small in comparison with the observed structures. Nevertheless valence angles are reproduced to an accuracy between 2° and 5°. Torsion angles do not appear to be biased. The accuracy with which they are reproduced is in the range of 3° and 8°. The accuracy of the force field is thus well within the range reported to be achievable by molecular modelling methods.[27,35,36]

Table 2. Agreement between calculated and experimental values of characteristic internal coordinates (distances [Å]; angles [°]

[a]	X-ray$_{av}$	mm2_rms$_{av}$	rmsd	mm2_int$_{av}$	rmsd
Rh−P	2.3	2.4	0.06	2.3	0.03
Rh−D	2.1	2.2	0.03	2.2	0.03
Rh−X			0.04		0.03
P−Rh−P	88.4	85.4	3.25	88.1	1.10
P−Rh−D	92.8	95.1	2.57	93.5	1.80
P−Rh−D	172.5	173.7	4.63	171.5	2.94
D−Rh−D	85.5	84.2	2.37	84.9	2.94
X−Rh−X			3.21		2.19
Rh−P−C3	114.0	116.2	2.90	114.2	1.86
Rh−P−C2	114.7	114.5	1.65	114.1	1.81
C2−P−C2	104.4	105.6	1.52	105.1	1.34
C2−P−C3	104.2	102.1	2.87	104.3	2.26
X−P−X			2.24		1.82
Rh−D−C2	85.5	84.2	2.37	84.9	2.94
P−Rh−D−C2	−93.6	−95.4	4.87	−94.1	2.57
Rh−P−C3−C3	−67.5	−67.6	4.00	−68.0	3.95
P−C3−C3−C3	−46.8	−44.7	7.95	−45.9	7.92
P−Rh−P−C3	−30.8	−31.5	4.02	−31.9	4.60

[a] The data in column X-ray$_{av}$ represent the average value of the corresponding internal coordinate over all eleven structures contained in the data basis. mm2_rms$_{av}$ and mm2_int$_{av}$ refer to the two sets of force field parameters reported in this paper. The numbers given under these column headers represent the mean of the corresponding internal coordinates for the calculated structures. The rms values given in each case represent the rms deviations for each class of internal coordinates as obtained by comparing calculated and experimentally observed values of each member of the corresponding set.

Grid Search Analysis of 1−3

A detailed analysis of the conformational space of molecules **1−3** is described in the following paragraphs. The analysis is based on the force field mm2_rms. To adequately scan the conformational space grids are defined as shown in Figure 6.

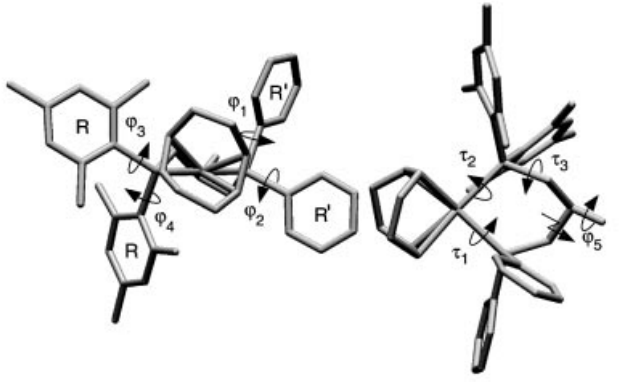

Compounds	PR_2	PR'_2		rotated fragments
1	$PMes_2$	PPh_2	τ_1	PR'_2CH_2
2	P(*o*–Tol)$_2$	PPh_2	τ_2	PR_2CH_2CHOH
3	DBP	P(*o*–Tol)$_2$	τ_3	CH_2CHOH

sense of positive rotation

ring closure bond

Figure 6. Conformational parameters of **1−3**. For a complete conformational search the actively driven conformational coordinates were chosen as shown. The four aryl rotations ($\varphi_1-\varphi_4$) were driven by using the rubberband protocol.[37] In order to relate the origin of the rotation to the coordination scaffolding the orientations where an aryl ring is parallel to the bisector of the P−Rh−P angle (vertical to the paper plane in the left hand side of the figure respectively horizontal in the right hand side of the figure) were defined as ±90°. The sense of rotation was taken as shown in the left hand diagram in Figure 6. By this definition an edge orientation is characterised by an φ value of ±90° while a face orientation corresponds to φ values of ±0°. The conformational coordinates ($\tau_1-\tau_3$) were as well actively driven using the ring closure bond protocol.[38] The rotational position of the OH group (φ_5) completes the coordinates of the eight dimensional conformational space.

The grid intervals for aryl rotations are set to the values in Table 3 upon detailed inspection of the experimentally determined structures of the relevant molecules. The resolutions were chosen such that any feasible rotational positions could be reached from the starting points. The conformations observed in the X-ray structures are selected as starting points in each case. To generate the starting conformations the 'rubberband' protocol was used which had already been found to be efficient with other compounds for which steric crowding did not allow for a direct rotation of their aryl groups.[37] The OH group was allowed to occupy the

Table 3. Definition and results of the grid search for compounds **1**−**3**

Compound	$\varphi_{1,2}$		$\varphi_{3,4}$		τ_{1-3}		φ_5		No. of starting geometries	No. of total minima	No. of minima in the range of $\Delta E \leq 50$ kJ·mol^{-1}
	range	step	range	step	range	step	range	step			
1	0°-180°	3	0°-180°	2	0°-360°	6	0°-360°	3	23328	91	82
2	0°-180°	2	0°-360°	3	0°-360°	6	0°-360°	3	23328	177	177
3	0°-360°	3	0°-360°	1	0°-360°	12	0°-360°	3	46656	92	92

three classical staggered positions. To construct chelate cycles with the appropriate torsion angles the 'ring closure' protocol was used.[38] Under this protocol the appropriate C−C bond is removed and reinstalled after adjusting the torsion angles to the selected values.

From the ten thousands of starting geometries (Table 3) force field minimisations lead to the same number of local minima, but many of them being the same. A comparison of these minimised structures leads to 91 independent minima for compound **1** and 92 of them in the case of **3**. For compound **2** there are 177 independent minima altogether reflecting the lower symmetry and the less strained situation in **2** as compared to the once in compounds **1** and **3**. From these local minima only a subset of 82, 177, and 92 is within a range of 50 kJ·mol^{-1} at or above the corresponding global minimum for compounds **1**−**3** in that sequence (Table 3).

To sort the conformations into classes with respect to the conformations adopted by their chelate cycles a Neural Network analysis of the Kohonen type was applied.[39] The six torsion angles characterising the conformations of the six-membered chelate cycles were used as the components of the input vectors. Self organisation of the 5 × 5 Kohonen network clearly revealed twelve individual classes in a two dimensional map.

The classes which lie within a energy window of 20 kJ·mol^{-1} are shown for **1** in Figure 7. It is seen that these classes conform to the standard classification of six-membered cycles. This means that the standard classification scheme is 'reinvented' by the Neural Network. If the different conformations are ranked according to the lowest energy calculated for the members of each specific class, the diagram as shown in Figure 7 results. It is satisfying to find that the λ and δ twist-boat conformations are at the lowest

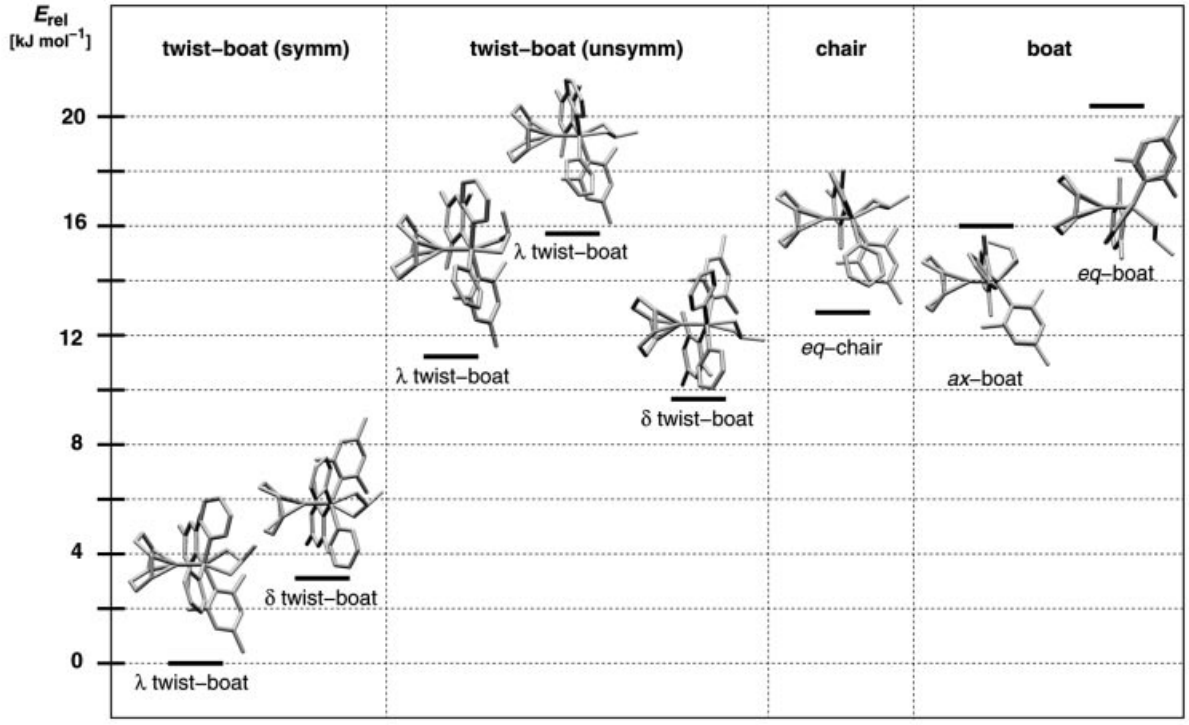

Figure 7. Classification of the conformations of the chelate cycle of **1**. The 91 independent local minima were sorted into the classes shown by Neural Network analysis. The energy scale refers to the lowest energy conformer in each class.

energy (Figure 7) since these are the conformations which are observed in the crystal of molecule **1**.

The same procedure when applied to the conformations which result as local energy minima from the analysis of **3** (Table 3) results in the diagram shown in Figure 8.

In this case the chair conformation − which almost exactly corresponds to the conformation of compound **3** in the solid state − has the lowest energy. It is however seen that other conformations are energetically almost equal to the one observed in the crystal such that the conformation

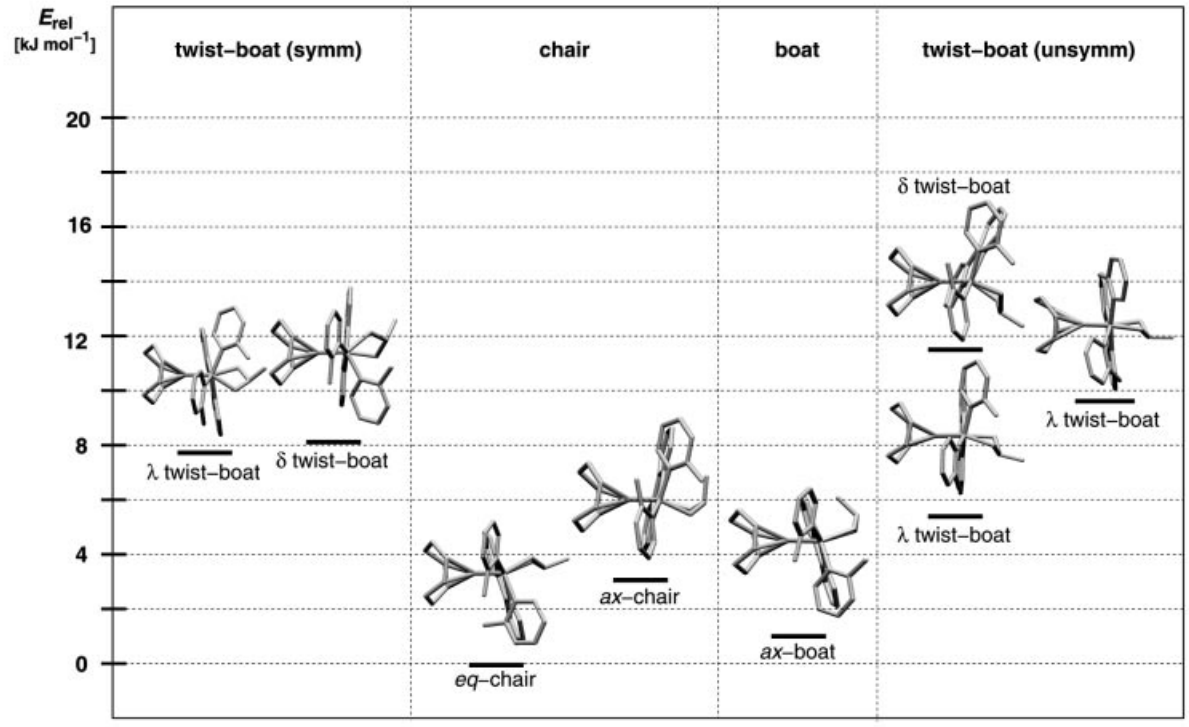

Figure 8. Classification of the conformations of the chelate cycle of **3**. The 92 independent local minima were sorted into the classes shown by Neural Network analysis. The energy scale refers to the lowest energy conformer in each class.

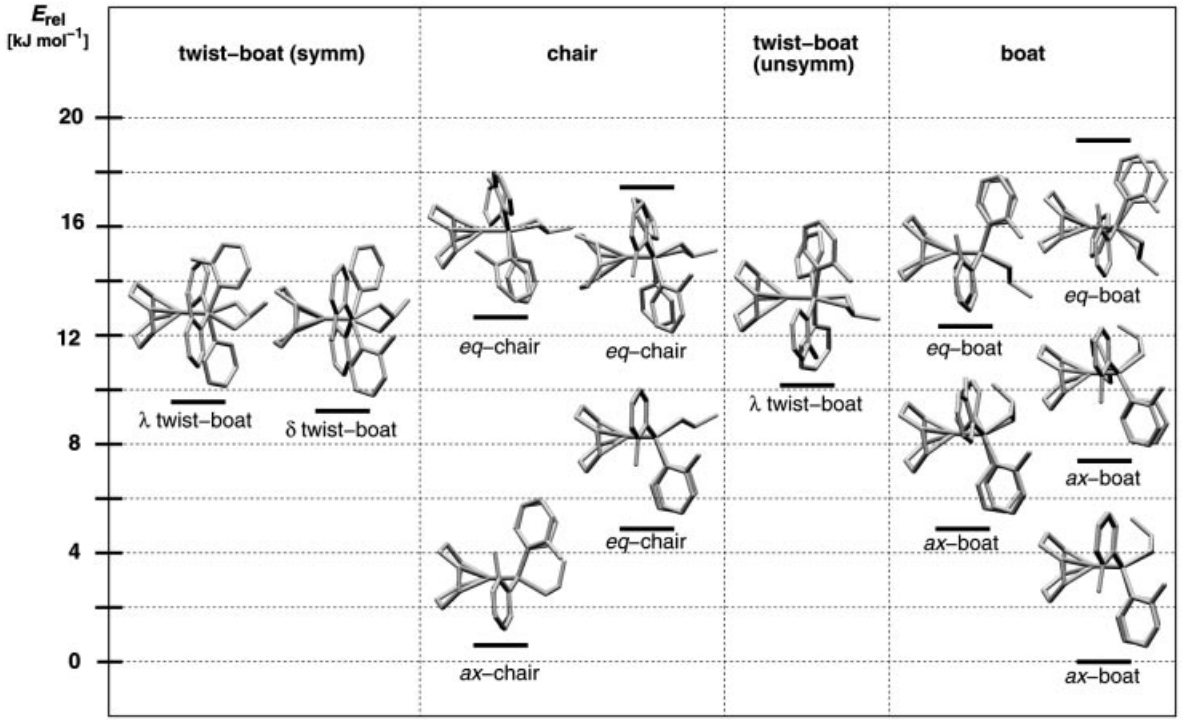

Figure 9. Classification of the conformations of the chelate cycle of **2**. The 177 independent local minima were sorted into the classes shown by Neural Network analysis. The energy scale refers to the lowest energy conformer in each class.

which should be found in the crystal cannot really be predicted. One would expect, however, that it should be one of the low energy molecular conformations which build up the crystal and it is in fact the one with the lowest calculated energy.

Figure 9 shows the same type of analysis for compound **2** where it is seen that the conformation observed in the crystal (chair, Figure 1) is amongst the conformations of the lowest energy of this compound but lies some 5 kJ·mol^{-1} above the global minimum.[40]

In comparing Figures 7−9 it is obvious that twist conformations are only preferred with **1** while **2** and **3** appear to prefer non-twisted conformations (chair or boat). Site differentiation by the two different PAr_2 groups is obviously largest for molecule **1** which prefers a twist conformation while the difference in the repulsive forces acting on the chelate cycle from the two different PAr_2 groups in **2** and **3** do not overcome the intrinsic preference of the more symmetric chair and boat conformations.

Energy − Reaction Pathway

With the approach taken in deriving force constants describing the potentials with respect to internal coordinates which involve the rhodium atom as a contributor there is no explicit reference to an energy scale (see paragraph Optimisation of Force Field Parameters). The reference is only implicit and the scale results by virtue of the scale intrinsic to the MM2* part of the force field. This part of the force field is thoroughly adapted to energy differences observed for organic molecules which means that it is capable of reproducing conformational pathways in organic chemistry not only with respect to structures but also with respect to relative energies. Since, with the molecules analysed, the interactions between their organic parts dominate it is expected that the force constants derived for the 'inorganic' part of the molecules by GA-optimisation will adapt to the major forces exerted by their organic part such that the scale of relative energies as calculated by the force field as a whole will be on scale with the observations. These expectations have been born out by similar analyses in related cases.[14−16] If the energies are on scale with the observations it must be possible to calculate conformationally relevant energies and to compare these with experimental values wherever available. The only molecule within the set studied for which experimental data relating to the relative stability of different conformers and to activation energies of conformational rearrangements are available is molecule **1**.[8] A more detailed analysis of the implications to be drawn from the force field calculations is therefore restricted to **1**.

An indication for the appropriateness of the energy scale is the finding (Figure 7) that the λ twist-boat conformation of **1** is calculated to be 3.1 kJ·mol^{-1} more stable than the δ twist-boat conformation. Experimentally it is observed that the energy difference between these conformers is $\Delta H =$ 3.4 kJ·mol^{-1} with the λ twist conformer being the more stable one.[8] The modelling approach hence predicts the correct sequence of relative stabilities and, even more, the calculated energy difference is in agreement with experiment.

NMR analysis shows that the conformational reaction pathway of the λ ⇄ δ interconversion of **1** is a complicated one.[8] It may or may not be accompanied by rotational rearrangements of the mesityl groups where on the other hand such mesityl rotations can only occur during λ ⇄ δ twist interchange.[8] If the force field approach is an appropriate one it should correctly predict this behaviour. To address this point contour maps were constructed in order to delineate the corresponding reaction path. To construct these maps with sufficient resolution with respect to the internal coordinates, which should best describe the pathway, grid points were calculated at a higher resolution (torsion angles $\tau_1-\tau_3$, rotational angles $\varphi_1-\varphi_4$, see Figure 6).

The diagrams (Figures 10−13, and 15) showing projections onto the τ_i/τ_j-planes ($i = 1-3$; $j = 2, 3$; $i \neq j$) were constructed in the following way: for any combination of the three τ-values (resolution in τ-space = 12°) the remaining coordinates ($\varphi_1-\varphi_5$) were allowed to refine in the same way as used in the global conformational search (see above). The lowest energy conformation from the stack of conformations thus obtained for each grid point was taken to represent the grid point in energy as well as in structure.

Figure 10 shows the isoenergy contour plot in a projection onto the τ_1/τ_3-plane. The λ and δ conformations which are the most stable conformations are shown on the left hand side of the diagram. A least energy pathway for the interconversion of these conformers along the τ_1/τ_3-plane is shown as a black line in the diagram. Individual conformations at the grid points corresponding to points along or close to this line are shown in sequence around the contour plot.

From this sequence of structural models it may be inferred that the rotation of the mesityl groups should occur at around $\tau_1 = 12°$; $\tau_3 = 24°$ (asterisk in the Figure 10) along the λ ⇄ δ interconversion pathway. It has already been stated that a whole stack of conformations has to be calculated for every grid point such that the one with the lowest energy can be chosen as a representative for each grid point. The conformations shown in Figure 10 are the ones having the lowest energy in each corresponding stack. For any conformation shown there is a pendant with an approximately opposite orientation of the mesityl groups, i.e. it is an orientation for which the aryl rotations ($\varphi_1-\varphi_4$ in Figure 6) are approximately equal in their absolute value but opposite in sign (compare $\mathbf{a_4}$ and $\mathbf{b_4}$ in Figure 10). The area around the point marked with an asterisk in Figure 10 is the one where the energy difference between these rotamers is the lowest one along the pathway i.e. less than 1 kJ·mol^{-1} against 10−80 kJ·mol^{-1} for the other grid points along the black line.

Figure 11 shows the isomerisation pathway in a projection onto the τ_1/τ_2- and τ_2/τ_3-planes. The values of the coordinates at which the concerted flip of the mesityl groups will occur are again (Figure 10) marked by an asterisk in each case.

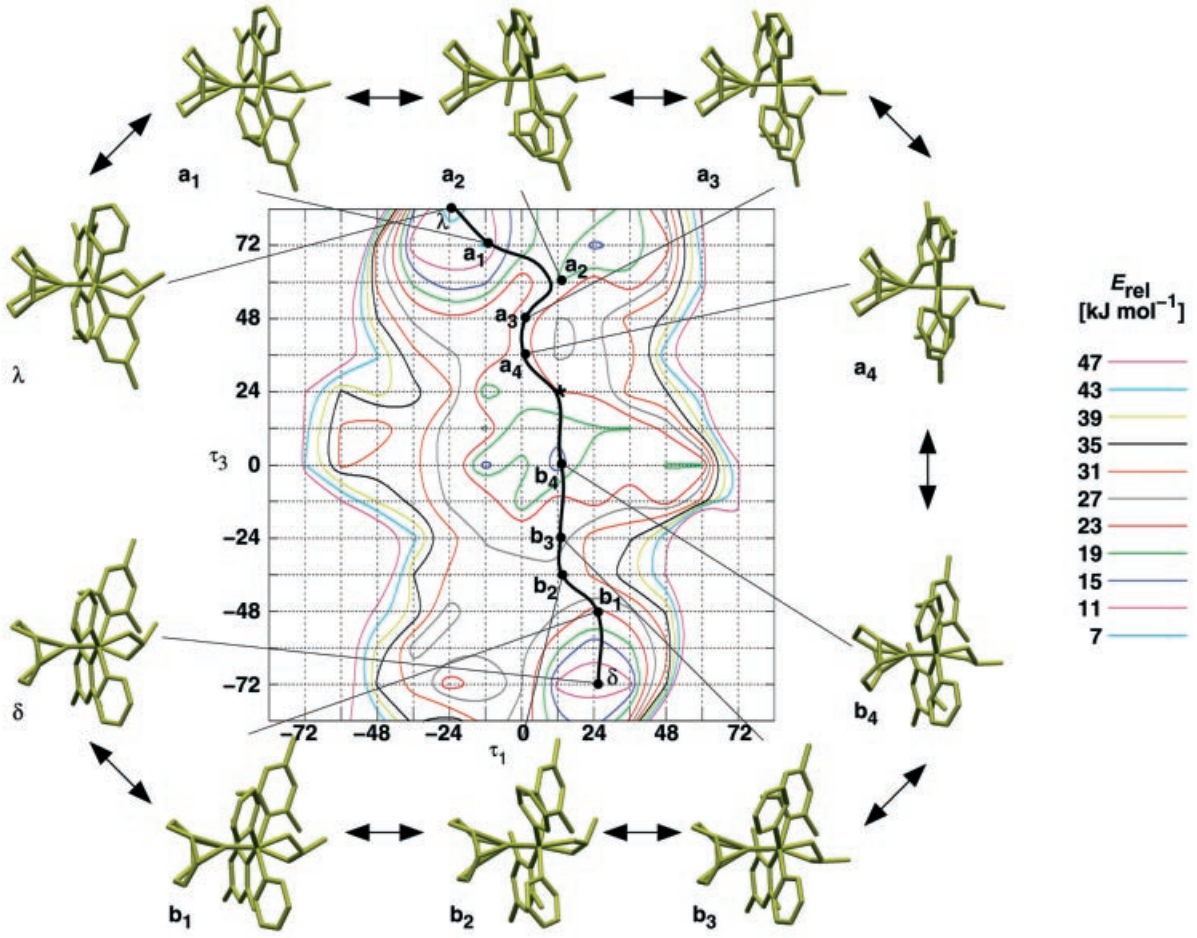

Figure 10. Projection of the energy hypersurface of **1** onto coordinates τ_1/τ_3, which characterise the conformation of the chelate cycle. To derive the contour plot the energy of the lowest energy conformation from each stack of conformations referring to each grid point was chosen as a representative. The reaction pathway (black line) was constructed such that it is a lowest energy route from the λ to the δ isomer. The conformations which characterise individual grid points are shown as molecular models around the contour plot. The conformations labelled **a** have an orientation of the aryl groups which corresponds in its sense to the one observed in the λ isomer. The conformations referenced by the label **b** have a different orientation which is similar to the one observed for the δ isomer. The region around the point marked with an asterisk is the one where the flip of the aryl rotation occurs.

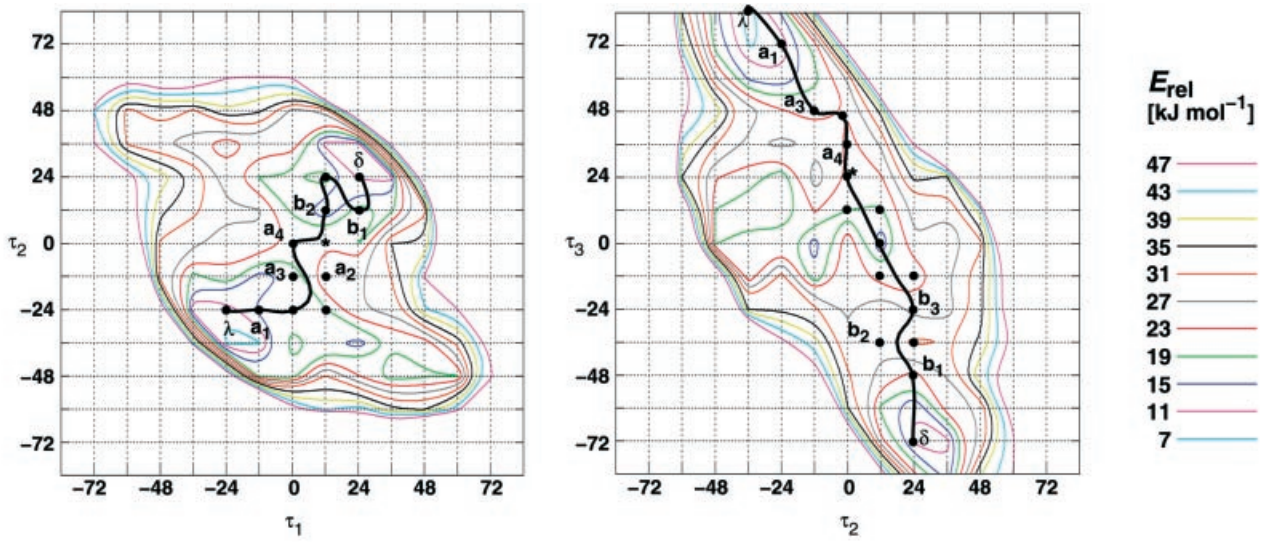

Figure 11. Projection of the energy hypersurface onto the τ_1/τ_2- and τ_2/τ_3-planes. The contour plots were constructed as described in the text and in the legend of Figure 10. The symbols **a**, **b**, λ, and δ refer to the conformations shown in Figure 10. The black lines indicate the projection of the reaction pathway for the $\lambda \rightleftarrows \delta$ isomerization. The asterisks pinpoint the region where the flip of the aryl rings occurs.

The reaction pathway, indicated by a black line in each case, corresponds to a smooth transition from one isomer into the other with all τ and φ values changing gradually along these curves. Only at the transition point marked by an asterisk there is a concerted flip of both mesityl groups by around 70° within a very short interval along the τ scale.

The kind of coupled rotation of the mesityl groups is evident from Figure 12 which shows the dependence of the energy on the rotational positions of the two mesityl groups. The diagram refers to the corresponding relative energies as calculated with τ_1, τ_2, and τ_3 fixed at 12°, 0°, and 24° respectively, i.e. at that point in τ-space (asterisk in Figures 10 and 11) which was found to induce the flip of the two mesityl groups.

It is found that the diagram shows pronounced minima at discrete positions which are labelled by **A** and **B**. The molecular models shown in Figure 12 illustrate the mutual arrangement of the mesityl groups. The conformation of the chelate cycle is the same in each case and corresponds to the specific triple of τ coordinates which was found to characterise the flip situation in τ space (asterisk in Figures 10 and 11). The energy minima labelled **A** correspond to a rotational position of the mesityl groups which is characteristic for the λ conformer. The labels **B** correspondingly refer to the rotational position of the mesityl groups as characteristic for the δ conformer. This means that all conformations labelled **A** will relax to the conformation of the λ isomer as soon as the τ values are allowed to refine. The conformations labelled **B** will correspondingly refine to the δ isomer upon relaxation of the constraints in τ space. Since the analysis of the τ-space diagrams (Figures 10 and 11) makes clear that any δ/λ transition and its reverse is necessarily accompanied by a concerted flip of the two mesityl groups the interpretation of Figure 12 is straightforward: A λ conformer (**A**) has two possibilities to change into a δ one. Starting from $\mathbf{A_1}$ as an example (Figure 12) there are two low energy pathways either to $\mathbf{B_1}$ or to $\mathbf{B_3}$. The rotational position of the mesityl groups corresponding to minima of type **B** is the one which corresponds to a δ isomer. This means that starting from the λ isomer ($\mathbf{A_1}$) a δ conformation can be reached on two ways: Either there will be a saddlepoint between $\mathbf{A_1}$ and $\mathbf{B_1}$ or a saddlepoint between $\mathbf{A_1}$ and $\mathbf{B_3}$. The barrier heights for these two types of transition are slightly different (Figure 12) while the energy of all the λ isomers (**A**) is necessarily the same but different from the energy of the δ isomers (**B**) which are again of equal energy for all members of the group. The only difference between energetically equal conformations such as $\mathbf{B_1}$ and $\mathbf{B_3}$ is then that the mesityl groups − even though they occupy fully equivalent positions in $\mathbf{B_1}$ and $\mathbf{B_3}$ as a whole − find themselves rotated by 180° on going from $\mathbf{B_1}$ to $\mathbf{B_3}$ (see colour coding of the conformations in Figure 12). The

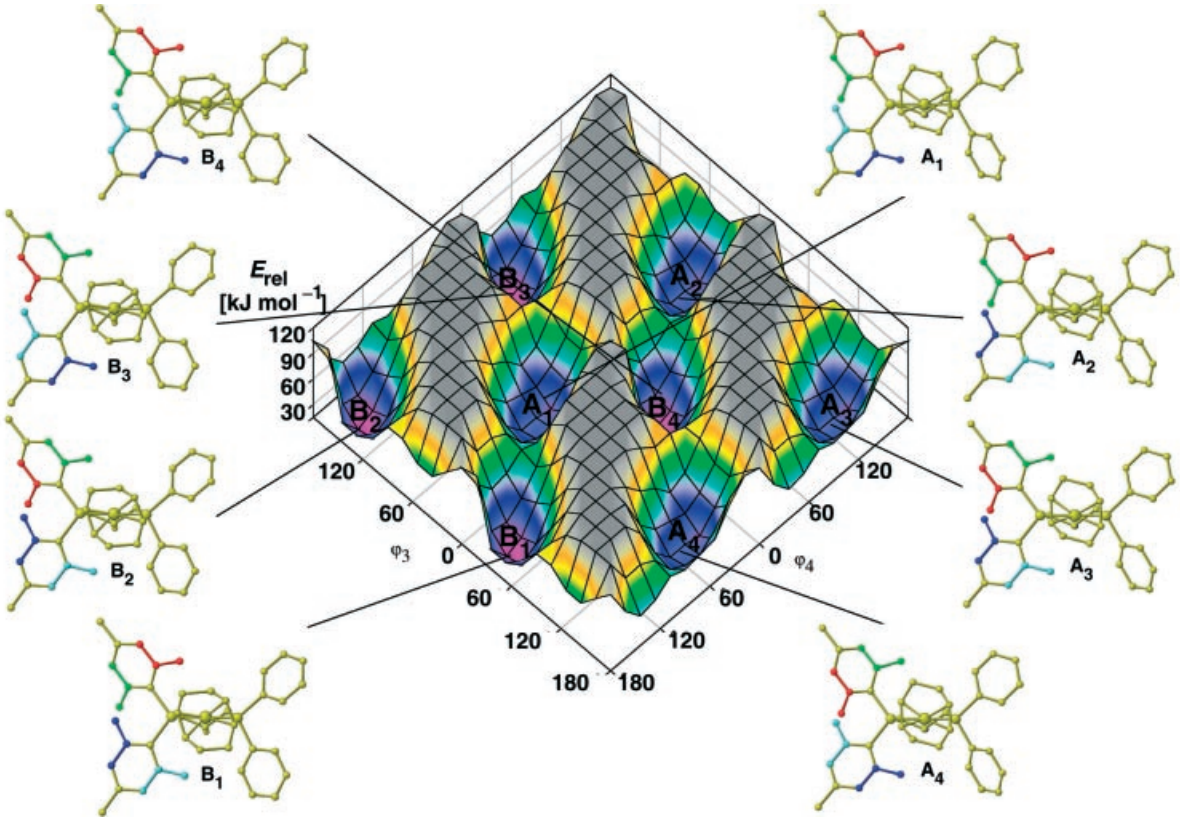

Figure 12. Energy diagram illustrating the pathways of rotational rearrangements of the $PMes_2$ entity of **1** during λ ⇄ δ isomerization. The translation symmetry of the graph is 180° in φ_3 and φ_4. The minima labelled **A** are characteristic for the λ isomer. The minima **B** likewise refer to the δ isomer. The molecular models $\mathbf{A_{1-4}}$ and $\mathbf{B_{1-4}}$ illustrate the rotational position of the mesityl groups for each of the eight minima shown. It is seen that the rotation of the mesityl groups at the $PMes_2$ entity is strictly coupled such that the groups have to rotate in mutually opposite sense.

conformations $\mathbf{B_1}$ and $\mathbf{B_3}$ are energetically fully equivalent; the ways however on which they are formed starting from $\mathbf{A_1}$ are different.

The energy diagram shown in Figure 12 has of course a translation period of 180°. The graph itself consists of four symmetrically independent unit cells. The fact that the mesi-

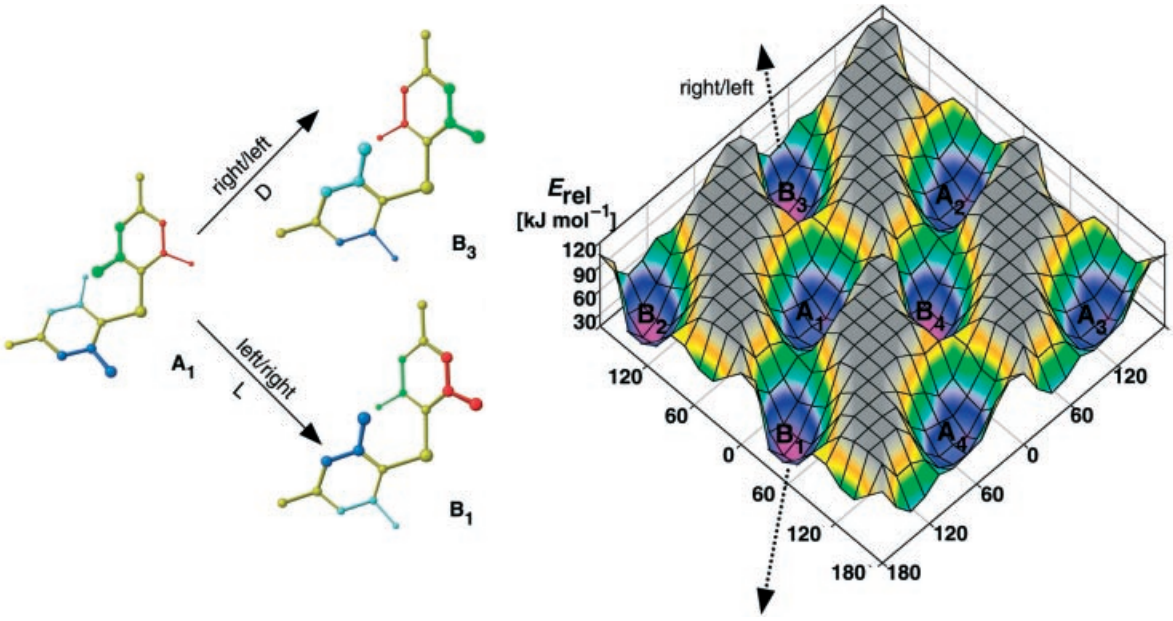

Figure 13. Illustration of the two energetically different pathways on which the $\lambda \rightleftarrows \delta$ isomerization of **1** may occur. The two pathways of $\lambda \rightleftarrows \delta$ isomerization are characterised by strictly coupled and countersense rotations of the mesityl groups at the $PMes_2$ entity. Depending on the sense of this coupled rotation different activation barriers have to be overcome. The two pathways labelled right/left (D) and left/right (L) are illustrated by molecular models.

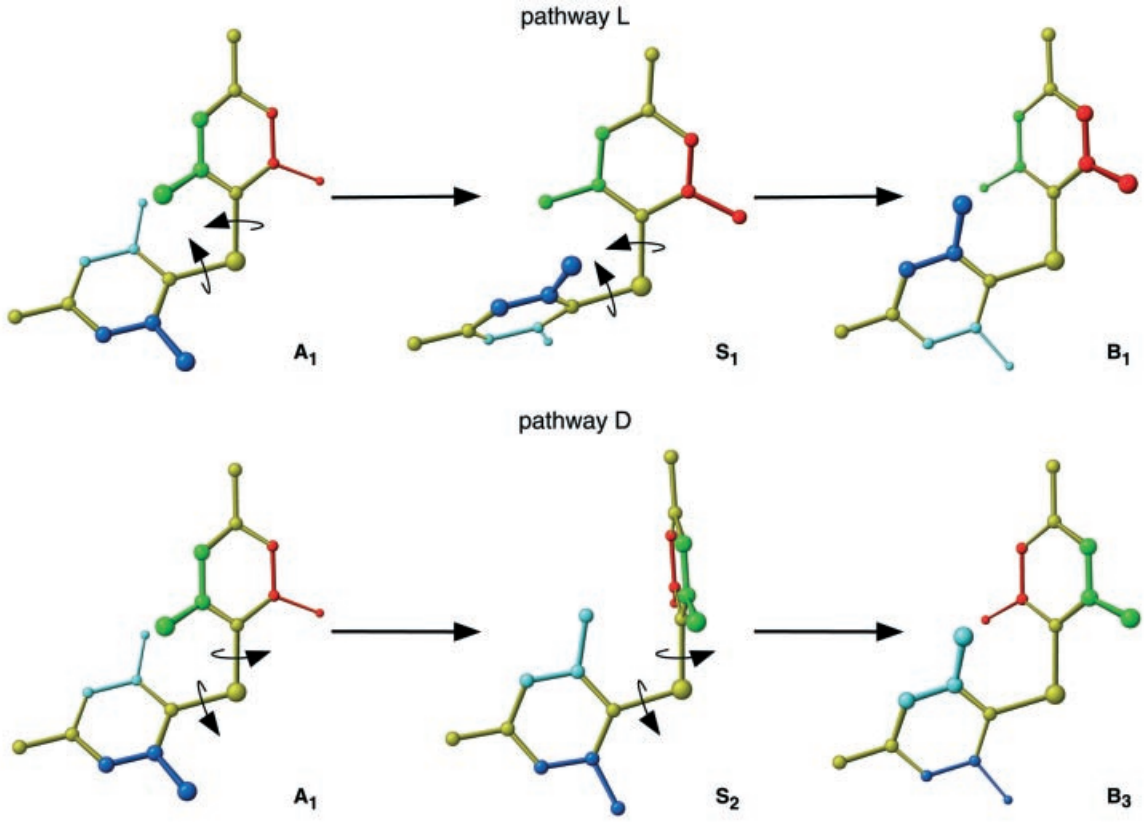

Figure 14. The one ring flip processes characterising the reorientation of the mesityl groups at the $PMes_2$ entity of **1** during $\lambda \rightleftarrows \delta$ isomerization. For the meaning of **A** and **B** see Figures 12 and 13. $\mathbf{S_1}$ and $\mathbf{S_2}$ correspond to the rotational positions of the mesityl groups at the saddlepoints (Figures 12 and 13).

tyl groups can only change their rotational positions as a strictly coupled pair is evident from Figure 12 as well. Only if the mesityl groups rotate in opposite sense the coupled rotation is allowed by low energy pathways. With the labelling scheme chosen $\mathbf{A_{(odd)}}$ can only interchange with $\mathbf{B_{(odd)}}$ and correspondingly $\mathbf{A_{(even)}}$ and $\mathbf{B_{(even)}}$ can interchange with each other. The corresponding reaction channels $\mathbf{B_1} \rightarrow \mathbf{A_1} \rightarrow \mathbf{B_3} \rightarrow \mathbf{A_3}$ are evident from Figure 12 where the minimum $\mathbf{A_3}$ is shown in a symmetrically equivalent position at the corner of the diagram (a phase shift in φ_3 by plus 180° will place $\mathbf{A_3}$ adjacent to $\mathbf{B_3}$). The channel $\mathbf{A_4} \rightarrow \mathbf{B_4} \rightarrow \mathbf{A_2} \rightarrow \mathbf{B_2}$ is likewise apparent in Figure 12 (a phase shift of −180° will place $\mathbf{B_2}$ adjacent to $\mathbf{A_2}$). A transition from a position on the pathway labelled by an uneven number subscript to any position on the pathway labelled by an even number subscript would correspond to either the rotation of just one mesityl group or to the coupled rotation of the two mesityl groups in the same rotational direction. Both possibilities are excluded by high potential barriers (grey barriers running vertical in Figure 12).

The rotational pathways taken by the mesityl groups upon $\lambda \rightleftarrows \delta$ isomerization are illustrated in Figure 13 in a different way. As an example the λ conformer $\mathbf{A_1}$ is taken as starting point. The mesityl groups labelled by φ_3 and φ_4 together with the phosphorus atom to which they are bonded are shown in a projection which keeps the $C_{ipso}-P-C_{ipso}$ fragment in the same orientation in each case (in the molecules themselves the pseudo-axial and pseudo-equatorial positions of the mesityl groups with respect to the coordination plane will exchange during the $\lambda \rightleftarrows \delta$ isomerization).

Following the pathway $\mathbf{A_1}$ to $\mathbf{B_3}$ (pathway D in Figure 12) the λ conformer transforms into the δ conformer such that φ_3 makes a clockwise rotation while φ_4 rotates in counterclock sense. This process needs a somewhat higher energy than the $\lambda \rightleftarrows \delta$ transformation from $\mathbf{A_1}$ to $\mathbf{B_1}$ (pathway L in Figure 13) which is accompanied by a counterclockwise rotation of φ_3 and a clockwise rotation of φ_4. These two pathways are labelled right/left for pathway D and left/right for pathway L respectively in Figure 13.

The two pathways L and D are illustrated in Figure 14 in yet another way. On the way from $\mathbf{A_1}$ to $\mathbf{B_1}$ (pathway L) the rotational arrangement corresponding to the saddlepoint (Figures 12 and 13) is the one shown ($\mathbf{S_1}$). The view taken in this Figure 14 is along the bisector of the P−Rh−P entity (Figure 6). The orientation is chosen such that one of the $P-C_{ipso}$ axes is vertical in each case in Figure 14.

The saddlepoint on the way from $\mathbf{A_1}$ to $\mathbf{B_3}$ (pathway D, Figures 12 and 13) is shown as well and labelled $\mathbf{S_2}$. It is

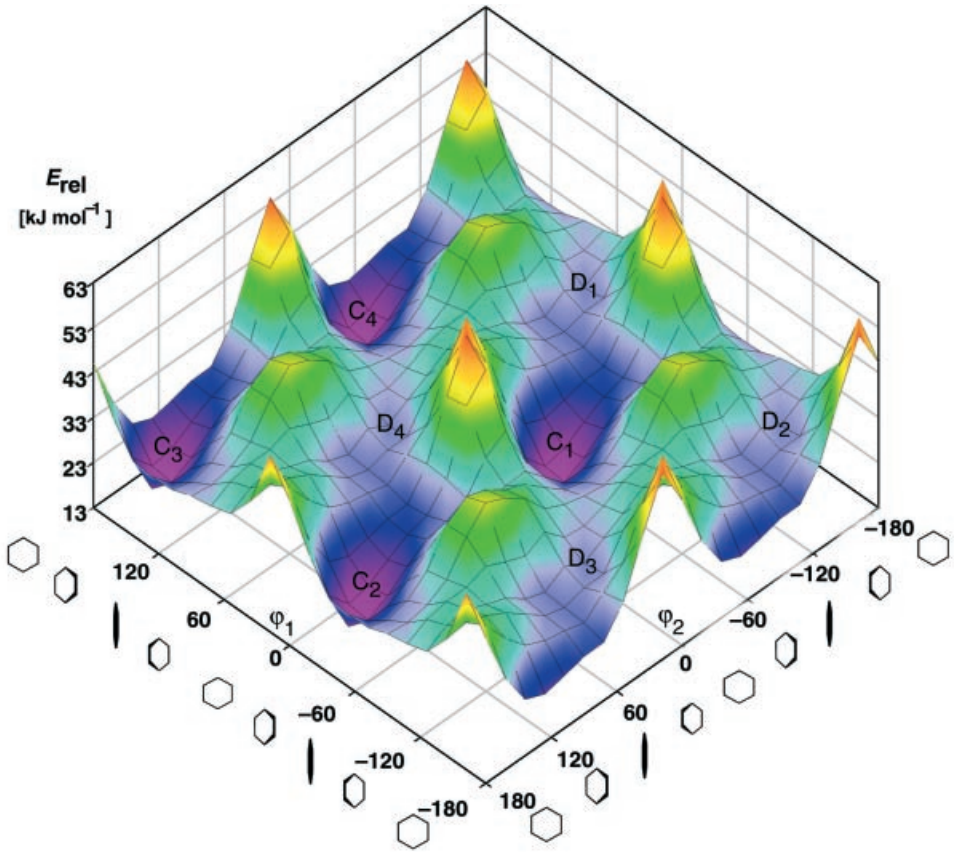

Figure 15. Energy diagram illustrating the ease of phenyl rotation at the PPh_2 group of **1**. The minima **C** are isoenergetic as are the flat minima **D**. The translation period of the graph is 180° in both axes. The energy scale is magnified with respect to the scale used in Figures 12 and 13. This larger magnification allows the illustration of the inherent asymmetry due to the chirality of **1**. The diagram is not symmetric with repect to the main diagonals (vertical in Figure 15).

seen that on both pathways the transition state corresponds to a situation where one of the aryl rings is almost vertical. The transitions thus correspond to a one ring flip process.[41]

The rotation of the phenyl groups at the PPh_2 entity is far less energy demanding than the rotation of the mesityl groups at the $PMes_2$ entity. The projection of the energy hypersurface onto the axes describing the rotation of the phenyl groups (φ_1, φ_2) is shown in Figure 15. This diagram is in principle analogous to the one shown in Figures 12 and 13. The energy scale and the energy profile are however quite different: In Figures 12 and 13 the barriers between the reaction channels (vertical reefs) are higher than 120 $kJ{\cdot}mol^{-1}$ (relative to the energy of the global minimum; Figures 12 and 13) and transition between different rotational positions is only energetically feasible along the two reaction channels.

The rotation of the phenyl groups on the other hand is far less restricted. The energy scale shown in Figure 15 is limited to 63 $kJ{\cdot}mol^{-1}$ with the highest barriers (orange) being covered within this range.

While a continuous reef separates the left hand and the right hand part of the Figures 12 and 13, in Figure 15 there are only isolated mountains and valleys between them. The positions of the minima **C** and **D** (Figure 15) are similar to the ones of **B** and **A** in Figures 12 and 13. This means that the low energy rotational positions of the aryl groups at the $PMes_2$ group and at the PPh_2 group are rather similar. There are however many energetically accessible pathways for concerted as well as for unconcerted phenyl rotations (Figure 15) while the mesityl groups can only rotate in a strictly concerted way (Figures 12 and 13). The barrier heights for the pathways reflecting the phenyl rotation are in the range of 12−15 $kJ{\cdot}mol^{-1}$ (Figure 15) while the barrier heights along the pathway of the strictly concerted rotation of the mesityl groups (pathways L and D, Figures 12 and 13) are in the range of 70−80 $kJ{\cdot}mol^{-1}$.

Force Field Model and Experimental Reality − Comparison of Results and Conclusion

The conformational behaviour of compounds **1**−**7** has been thoroughly analysed by NMR methods.[8] For compound **1** the quantitative details relating to the relative stability of its isomeric forms and to the pathways of isomerization and the activation enthalpy of this process are all available. It is found that the λ form of **1** is by 3.4 $kJ{\cdot}mol^{-1}$ more stable than its δ form.[8] Force field analysis calculates this energy difference as 3.1 $kJ{\cdot}mol^{-1}$ in almost exact numerical agreement (Figure 16). NMR exchange spectroscopy reveals that there are two different pathways for the isomerization of **1**.[8] Both pathways are characterised by a coupled rotation of the mesityl groups at the $PMes_2$ entity of **1**. The only difference between these two pathways is the opposite sense of this strictly coupled rotation.[8] The activation enthalpy for the enantiomerisation process as a whole is found to be $\Delta H^{\#}$ = 64.4 $kJ{\cdot}mol^{-1}$.[8] Force field calculations of **1** show that there are two pathways for λ ⇄ δ isomerization which comprise the strictly coupled countersense rotation of the mesityl groups at the $PMes_2$ entity and which differ only in the sense of rotation. The calculated activation enthalpy of the lower energy pathway is 69.1 $kJ{\cdot}mol^{-1}$, again in close nu-

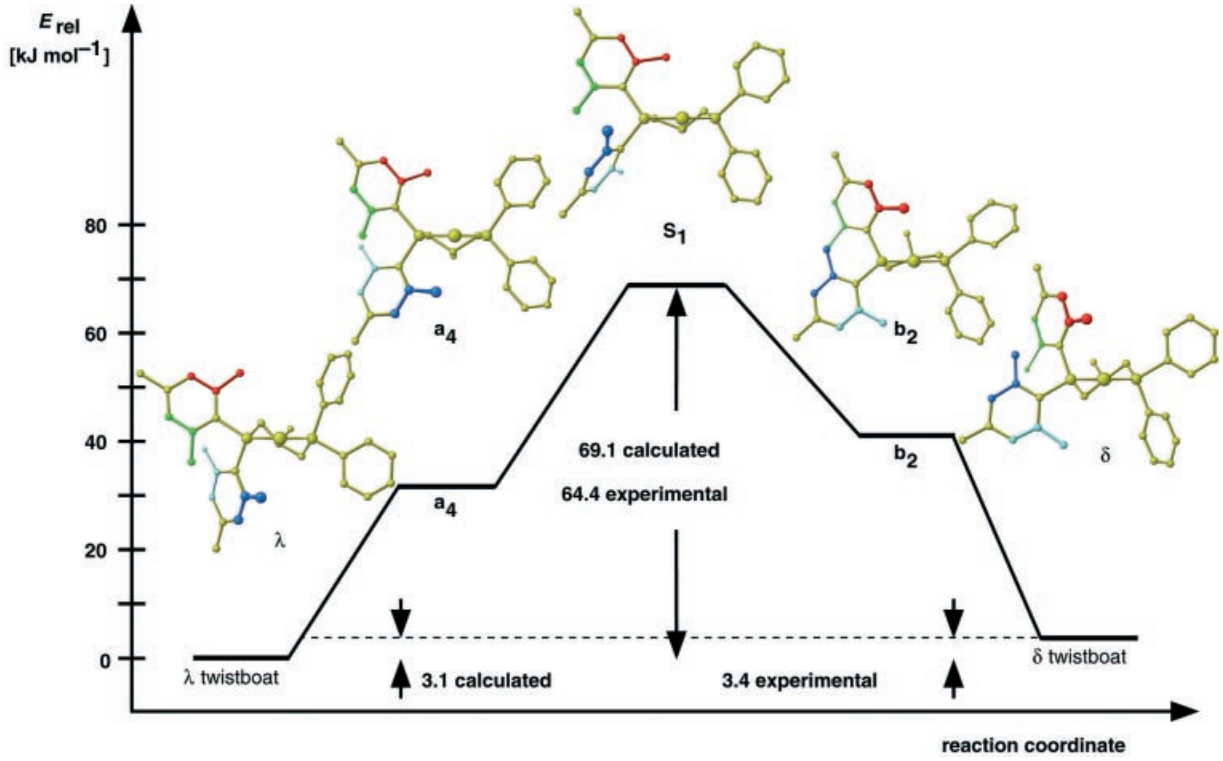

Figure 16. Comparison of experimental and calculated results for the λ ⇄ δ isomerization of **1**.

merical agreement with the experimental value (Figure 16). This type of quantitative and qualitative agreement between calculation and experiment lends quite some credit to the calculation procedures as reported. The force field calculations identify the conformation of the chelate ring at the saddlepoint as an unsymmetrical twist conformation. Starting from the λ isomer this transition state geometry is reached via a halfboat conformation (**a**$_4$ in Figure 16). Starting from the δ isomer a twist conformation (**b**$_2$ in Figure 16) is the intermediate.

It appears that the approach taken in deriving a force field model is a very promising one. The optimisation of the force field parameters on the basis of as many solid state structures as available for a class of compound had already been shown to lead to models of high predictive power.[14−16] The case studied here is the most complicated one of the ones analysed by this method so far and at the same time the one for which pathways and energies have been experimentally determined to the maximum possible extent.[8] It is highly satisfying to observe that the model is capable of predicting the types of conformational rearrangement processes as well as the energy differences associated with them.

Experimental Section

Force Field Calculations

The force field program used is based on the program set YAMMP[23] written by R. K. Z. Tan et al. in "C" which is available as a public domain source code.[42] The force field potentials were adapted to the units used in MacroModel MM2*.[21] Data transfer between MacroModel and YAMMP was accomplished by appropriate converters and YAMMP was embedded in a number of shells which make it available at different types of single processor machines (Pentium, SGI) and parallel computing systems (Parsytec GC, CRAY T3E).

The rms deviation between two structural models was calculated as the square root of the sum of the squares of the deviations between all n corresponding pairs of atoms divided by the square root of n (Hydrogen atoms were included in these calculations during GA optimisation). An overlay of the two structures was computed by a least-squares fitting procedure based on a program of D. Heisenberg[43] and implemented into YAMMP by K. Allinger.[14]

The following expressions were used for the potential energy:

Bond Length Deformation:

$$E(r) = 1/2\,k((r-r_0)^2 - (r-r_0)^3) \quad (1)$$

where r_0 represents the ideal bond length (minimum of the curve) and r represents the actual distance. This potential curve has a artificial maximum at large ($r-r_0$) values. For such large values only the quadratic term is used.

Valence Angle Deformation:

$$E(\alpha) = 1/2\,k((\alpha-\alpha_0)^2 + k'(\alpha-\alpha_0)^6) \quad (2)$$

α_0 and α have a similar meaning as r_0 and r above. The force constants k ank k' refer to the contributions of the harmonic and the unharmonic parts of the potential function to the energy.

Torsion Angle Deformation:

$$E(\tau) = k_{t1}(1+\cos\tau) + k_{t2}(1-\cos(2\tau)) + k_{t3}(1+\cos(3\tau)) \quad (3)$$

The variable τ describes the torsion angle. k_{t1}, k_{t2}, and k_{t3} are the force constants describing potential terms with twofold, fourfold and sixfold symmetry in this series.

π-Bonds: π-bonding was incorporated by defining a dummy atom D at the centre of the coordinated double bond (Figure 3). The position of the olefinic carbon atoms was then expressed as a function of r_d, α, β, γ, and τ (Figure 3). The terms needed in a molecular mechanics calculation are however of the type $\delta E/\delta x$ (x being any coordinate of any atom in real space) and not of the type $\delta E/\delta p$ (p being any internal coordinate). The potentials on the other hand are defined as $E = f(p)$ and it is necessary therefor to transform $\delta E/\delta p$ into $\delta E/\delta x$. This problem is solved for the standard set of conformational coordinates (distance, angle, torsion angle ...) in any standard molecular mechanics program. It is not incorporated, however, for parameters such as r_d, α, β, γ, and τ which were used to define a π bond (Figure 3). In principle the solution is given by differential calculus by $\delta E/\delta x = (\delta E/\delta p)\cdot(\delta p/\delta x)$. With the parameters r_d, α, β, γ, and τ the application of this rule is rather tedious. For this reason and since the corresponding expressions cannot be found in the literature the results are given here for the derivatives with respect to the x-coordinate in each case. The derivatives for the other coordinates are easily obtained from these expressions by cyclic permutation.

If a_x represents the x coordinate of the real atom (rhodium in Figure 3) and d_x the x coordinate of the dummy atom (D in Figure 3) the expression relating to r_d is:

$$\delta E/\delta d_x = -\delta E/\delta a_x = k\Delta r_d \cdot (a_x - d_x)/|r_d| \quad (4)$$

The term Δr_d means ($|\vec{r_0}| - |\vec{r}|$ where $|\vec{r}|$ is the distance r_d and $|\vec{r_0}|$ is the distance at the minimum of the potential function.

In order to derive the expressions relating to α, β, and γ (Figure 3) the following definition is used (Figure 17).

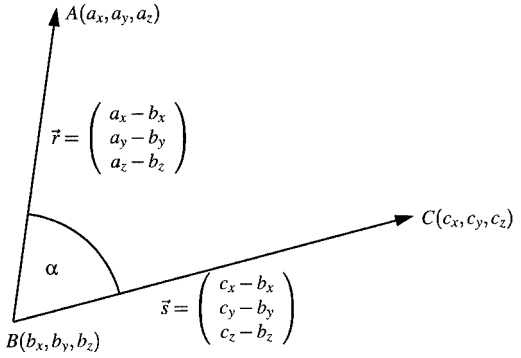

Figure 17. Definitions used in calculating derivatives with respect to angles.

If the potential function $E(\alpha) = {}^1/_2k\cdot[(\alpha - \alpha_0)^2 + k_{unh}\cdot(\alpha - \alpha_0)^6]$ is defined as above the derivatives with respect to the x coordinates of the points A, B, and C are:

$$\frac{\delta E(\alpha)}{\delta a_x} = k_{angle}\cdot\Delta\alpha\cdot\left(1+3\cdot k_{unh}\cdot(\Delta\alpha)^4\right)\cdot\frac{-1}{\sin\alpha} \cdot\frac{|\vec{r}|^2\cdot(c_x-b_x)-\vec{r}\cdot\vec{s}\cdot(a_x-b_x)}{|\vec{r}|^3\cdot|\vec{s}|}$$

$$\frac{\delta E(\alpha)}{\delta b_x} = k_{angle}\cdot\Delta\alpha\cdot\left(1+3\cdot k_{unh}\cdot(\Delta\alpha)^4\right)\cdot\frac{-1}{\sin\alpha} \cdot\frac{\vec{r}\cdot\vec{s}\cdot|\vec{s}|^2\cdot(a_z-b_x)-(a_x-2b_x+c_x)\cdot|\vec{r}|^2\cdot|\vec{s}|^2+\vec{r}\cdot\vec{s}\cdot|\vec{r}|^2\cdot(c_x-b_x)}{|\vec{r}|^3\cdot|\vec{s}|^3} \quad (5)$$

$$\frac{\delta E(\alpha)}{\delta c_x} = k_{angle}\cdot\Delta\alpha\cdot\left(1+3\cdot k_{unh}\cdot(\Delta\alpha)^4\right)\cdot\frac{-1}{\sin\alpha} \cdot\frac{|\vec{s}|^2\cdot(a_x-b_x)-\vec{r}\cdot\vec{s}\cdot(c_x-b_x)}{|\vec{r}|\cdot|\vec{s}|^3}$$

The term $\Delta\alpha$ means ($\alpha - \alpha_0$) in each case (see above).

For analysing $\delta E/\delta\tau$ (Figure 3) the definitions shown in Figure 18 are used.

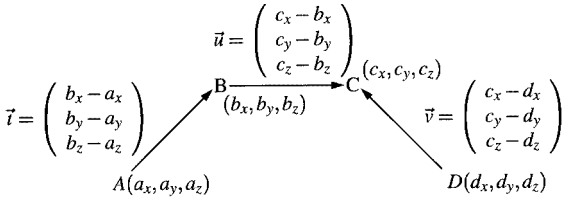

Figure 18. Definitions used in calculating derivatives with respect to torsion angles.

Two additional vectors are defined as:

$$\vec{r} = \vec{t}\times\vec{u} \text{ and } \vec{s} = \vec{u}\times\vec{v} \quad (6)$$

With a_x, b_x, c_x, and d_x being the x coordinates of the points A, B, C, and D in that sequence the following expressions result:

$$\frac{\delta E(\tau)}{\delta a_x} = \left(k_{t1}\cdot(1+\cos\tau)+k_{t2}\cdot(2\cos^2\tau-1)+k_{t3}\cdot(4\cos^3\tau-3\cos\tau)\right) \cdot\frac{|\vec{r}|\cdot|\vec{s}|\cdot(u_z s_y-u_y s_z)-\vec{r}\cdot\vec{s}\cdot\frac{|\vec{s}|}{|\vec{r}|}\cdot(r_y u_z-r_z u_y)}{|\vec{r}|^2\cdot|\vec{s}|^2}$$

$$\frac{\delta E(\tau)}{\delta b_x} = \left(k_{t1}\cdot(1+\cos\tau)+k_{t2}\cdot(2\cos^2\tau-1)+k_{t3}\cdot(4\cos^3\tau-3\cos\tau)\right) \cdot\left(\frac{|\vec{r}|\cdot|\vec{s}|\cdot(s_y(-t_z+u_z)+r_y v_z+s_z(-u_y+t_y)-r_z v_y)}{|\vec{r}|^2\cdot|\vec{s}|^2} -\frac{\vec{r}\cdot\vec{s}\cdot\left(\frac{|\vec{r}|}{|\vec{s}|}\cdot(r_y(u_z-t_z)+r_z(-u_y+t_y))+\frac{|\vec{r}|}{|\vec{s}|}\cdot(s_y v_z-s_z v_y)\right)}{|\vec{r}|^2\cdot|\vec{s}|^2}\right) \quad (7)$$

$$\frac{\delta E(\tau)}{\delta c_x} = \left(k_{t1}\cdot(1+\cos\tau)+k_{t2}\cdot(2\cos^2\tau-1)+k_{t3}\cdot(4\cos^3\tau-3\cos\tau)\right) \cdot\left(\frac{|\vec{r}|\cdot|\vec{s}|\cdot(r_y(-v_z+u_z)+s_y t_z+r_z(-u_y+v_y)-s_z t_y)}{|\vec{r}|^2\cdot|\vec{s}|^2} -\frac{\vec{r}\cdot\vec{s}\cdot\left(\frac{|\vec{r}|}{|\vec{s}|}(s_y(u_z-v_z)+s_z(v_y-u_y))+\frac{|\vec{r}|}{|\vec{s}|}\cdot(r_y t_z-r_z t_y)\right)}{|\vec{r}|^2\cdot|\vec{s}|^2}\right)$$

$$\frac{\delta E(\tau)}{\delta d_x} = k_{t1}\cdot(1+\cos\tau)+k_{t2}\cdot(2\cos^2\tau-1)+k_{t3}\cdot(4\cos^3\tau-3\cos\tau) \cdot\frac{|\vec{r}|\cdot|\vec{s}|\cdot(u_y r_z-u_y r_y)-\vec{r}\cdot\vec{s}\cdot\frac{|\vec{r}|}{|\vec{s}|}\cdot(s_z u_y-s_y u_z)}{|\vec{r}|^2\cdot|\vec{s}|^2}$$

Optimisation by GA

The procedures already explicitly described elsewhere[14] based on the use of the program GAPAO which itself uses functions of the

Table 4. Optimised force constants

(a) Bond Stretching[a]	parameter set mm2_rms r_0 [Å]	k_b [mdyn·Å^{-1}]	parameter set mm2_int r_0 [Å]	k_b [mdyn·Å^{-1}]
Rh−P	2.310	0.625	2.310	1.357*
Rh−D	2.140	1.000	2.140	1.267*
(b) Angle Bending	parameter set mm2_rms α_0 [°]	k_a [mdyn·rad^{-2}]	parameter set mm2_int α_0 [°]	k_a [mdyn·rad^{-2}]
P−Rh−P	88.6	0.600	93.0*	0.800*
P−Rh−D	93.5/175.8	0.500	93.5/175.8	0.047*
D−Rh−D	90.0	0.100	91.667*	0.500*
Rh−P−C3	118.133*	0.467*	117.067*	0.677*
Rh−P−C2	112.800*	0.967*	113.200*	0.633*
C2−P−C2	103.600*	1.200*	103.571*	0.700*
C2−P−C3	99.194*	0.867*	103.143*	0.533*
Rh−D−C2	90.000	0.250	90.000	1.000*
(c) Torsion	parameter set mm2_rms k_{t2} [kcal·mol^{-1}]	k_{t3} [kcal·mol^{-1}]	parameter set mm2_int k_{t2} [kcal·mol^{-1}]	k_{t3} [kcal·mol^{-1}]
P−Rh−D−C2	0.000*	0.000	−1.000*	0.000

[a] Parameter set mm2_rms was obtained by calculating the fitness on the basis of the distance between pairs of atoms, one atom belonging to the experimentally observed structure and the constitutionally equivalent atom belonging to the calculated structure. Parameter set mm2_int was obtained by evaluating the fitness on the basis of the internal coordinates as shown. Only parameters marked with an asterisk were refined. Harmonic potentials were used for the bond length deformation. The unharmonic term k_{unh} of the valence angle deformation (see text) was set at $k_{unh} = 0.754$ rad^{-4} throughout.

PGA-Genetic Algorithm Package[44] were applied. These functions are fully parallelised and are based on the Message Passing Interface Library[45] and thus GAPAO runs in single processor as well as in parallel processor environments.

The force constants as derived by optimisation on the basis of eleven structures are shown in Table 4.

Conformation Analysis

The procedure used was similar to the one described in detail elsewhere.[15] Two dimensional and pseudo-three dimensional contour plots were produced by using the program *SigmaPlot*.[46] Neural Network analyses were calculated and visualised by the program kmap.[47] The calculations were performed by using the modified program YAMMP as a minimizer and a shell around it which allowed to run the program on parallel processor environments. The standard program YAMMP was augmented by a part, written in "C", implementing a grid search algorithm. All calculations were performed on a Cray T3E.

Acknowledgments

Financial support by the German Science Foundation (DFG HU 151/24-1 and DFG HU 151/29-1), the Fonds der Chemischen Industrie and the Graduiertenkolleg "Selektivität in der organischen und metallorganischen Synthese und Katalyse" is gratefully acknowledged. The computations were made possible by grants of computing time at PARSYTEC (IWR Heidelberg) and CRAY [John von Neumann Institut (NIC)] parallel computing environments. We are indebted to J. Gasteiger, Erlangen, for the allowance to use the program kmap written by the Erlangen group.

[1] U. Burkert, N. L. Allinger, *Molecular Mechanics*, ACS monograph, Washington, **1992**.
[2] E. Juaristi, *Introduction to Stereochemistry & Conformational Analysis*, Wiley Interscience, **1991**.
[3] P. Comba, T. W. Hambley, Molecular Modelling of Inorganic Compounds, VCH Weinheim, **1995**.
[4] C. R. Landis, D. M. Root, T. Cleveland, in: *Reviews in Computational Chemistry*, Vol. 6 (Eds.: K. B. Lipkowitz, D. B. Boyd), VCH Publishers, Inc., New York, **1995**, 73−148.
[5] B. J. Hay, *Coord. Chem. Rev.* **1993**, *126*, 177−236.
[6] [6a] *Discover User Guide*, Versions 2.9.7 & 95.0/3.00, Biosym/MSI, **1995**. [6b] S. Barlow, A. L. Rohl, S. Shi, C. M. Freeman, D. O'Hare, *J. Am. Chem. Soc.* **1996**, *118*, 7578−7592. [6c] N. Jäger, U. Schilde, *Struct. Chem.* **1998**, *9*, 77−93.
[7] D. M. Root, C. R. Landis, T. Cleveland, *J. Am. Chem. Soc.* **1993**, *115*, 4201−4209.
[8] A paper presenting quantitative thermodynamic and kinetic data of the conformational rearrangements of diphosphane chelate compounds including **1** as deduced by NMR techniques is published aside: A. Frick, V. Schulz, G. Huttner, *Eur. J. Inorg. Chem.* **2002**, 3129−3147, following paper.
[9] T. W. Hambley, *J. Comput. Chem.* **1987**, *8*, 651−657.
[10] J. R. Gollogly, C. J. Hawkins, *Inorg. Chem.* **1972**, 156−161.
[11] S. Beyreuther, J. Hunger, G. Huttner, S. Mann, L. Zsolnai, *Chem. Ber.* **1996**, *129*, 745−757.
[12] G. Huttner, S. Beyreuther, J. Hunger, in: *Software-Entwicklung in der Chemie 10* (Ed.: J. Gasteiger), GDCH, Frankfurt am Main, **1996**, 201−207.
[13] J. Hunger, S. Beyreuther, G. Huttner, *Mol. Model.* **1996**, 2, 257−258.
[14] J. Hunger, S. Beyreuther, G. Huttner, K. Allinger, U. Radelof, L. Zsonai, *Eur. J. Inorg. Chem.* **1998**, 693−702.
[15] S. Beyreuther, J. Hunger, S. Cunskis, T. Diercks, A. Frick, E. Planker, G. Huttner, *Eur. J. Inorg. Chem.* **1998**, 1641−1653.
[16] S. Beyreuther, A. Frick, J. Hunger, G. Huttner, B. Antelmann, P. Schober, R. Soltek, *Eur. J. Inorg. Chem.* **2000**, 597−615.
[17] D. E. Goldberg, *Genetic Algorithms in Search, Research and Machine Learning*, Addison-Wesely, New York, **1989**.
[18] J. Devillers (Ed.), *Genetic Algorithms in Molecular Modelling*, Academic Press, San Diego, **1996**.
[19] R. Judson, in: *Reviews in Computational Chemistry*, Vol. 10 (Eds.: K. B. Lipkowitz, D. B. Boyd), VCH Publishers, Inc., New York, **1997**, 1−73.
[20] J. Karas, G. Huttner, K. Heinze, P. Rutsch, L. Zsnolnai, *Eur. J. Inorg. Chem.* **1999**, 405−420.
[21] The mm2 force field as implemented in MacroModel 5.0 (mm2*) has been used throughout (see: F. Mohamadi, N. G. J. Richards, W. C. Guida, R. Liskamp, M. Lipton, C. Caufield, G. Chang, T. Hendrickson, W. C. Still, *J. Comp. Chem.* **1990**, *11*, 440−467).
[22] N. L. Allinger, *J. Am. Chem. Soc.* **1977**, *99*, 8127−8134.
[23] R. K.-Z. Tan, S. C. Harvey, *J. Comp. Chem.* **1993**, *14*, 455−470.
[24] T. N. Doman, C. R. Landis, B. Bosnich, *J. Am. Chem. Soc.* **1992**, *114*, 7264−7272.
[25] B. Bosnich, *Chem. Soc. Rev.* **1994**, 387−395.
[26] W. F. van Gunsteren, R. Boelens, R. Kaptein, R. M. Scheek, E. R. P. Zuiderwig, *Molecular Dynamics and Protein Structure* (Ed.: J. Hermans), Polycrystal Book Service: West Springs, IL, **1985**, p. 92.
[27] V. S. Allured, C. M. Kelly, C. R. Landis, *J. Am. Chem. Soc.* **1991**, *113*, 12−20.
[28] The conventional binary code has the disadvantage that occasionaly more than one bit has to be changed in going from the binary representation of n to $n + 1$ (cf.: $n = 3$, code = 011; $n = 4$, code = 100). In applying Genetic Algorithms this would mean that it is more probable to change a 4 into a 5 (100; 101) than it is to change a 3 into a 4. 'Grey coding' avoids this problem by assigning a binary code such that only one bit has to be inverted in going from n to $n + 1$ throughout.
[29] J. H. Holland, *Adaption in Natural and Artifical Systems*, MIT Press, Cambridge, MA, **1992**.
[30] D. E. Goldberg, *Genetic Algorithms in Search, Research and Machine Learning*, Addison-Wesley, New York, **1989**.
[31] J. Devillers (Ed.), *Genetic Algorithms in Molecular Modelling*, Academic Press, San Diego, **1996**.
[32] R. Judson, in: *Reviews in Computational Chemistry, Vol. 10* (Eds.: K. B. Lipkowitz, D. B. Boyd), VCH Publishers, Inc. New York, **1997**, 1−73.
[33] D. Wienke, C. B. Lucasius, G. Kateman, *Anal. Chim. Acta* **1992**, *265*, 211−225.
[34] The structure contains one molecule CH_2Cl_2 and half a molecule Et_2O per formula unit. Both of these solvate molecules as well as PF_6^- counterions are disordered. Relatively short contacts between the hydroxy oxygen of the ligand and some of the fluorine substituents of the counterion PF_6^- (2.8 Å) and some of the chlorine atoms of the dichloromethane solvate (3.3 Å) indicate that the structure of the ligand might be biased by these contacts.
[35] B. P. Hay, *Coord. Chem. Rev.* **1993**, *126*, 177−236.
[36] P. Comba, *Coord. Chem. Rev.* **1993**, *123*, 1−48.
[37] J. S. Giovannetti, C. M. Kelly, C. R. Landis, *J. Am. Chem. Soc.* **1993**, *115*, 4040−4057.
[38] M. Lipton, W. C. Still, *J. Comp. Chem.* **1988**, *9(4)*, 343−355.
[39] T. Kohonen, *Self-Organization and Associative Memory*, 2nd. ed., Springer Verlag, Berlin **1988**.
[40] It is often observed that conformations found in the crystal do not correspond to the conformation of the global energy minimum but have conformations for which the calculated energies are some few kJ·mol^{-1} higher. In the example analysed crystal forces are weak throughout but obviously strong enough to overcome some few kJ·mol^{-1} (see ref[15]).
[41] [41a] D. A. V. Morton, A. G. Orpen, *J. Chem. Soc., Dalton*

Trans. **1992**, *4*, 641−653. [41b] K. Mislow, *Acc. Chem. Res.* **1976**, *9*, 26−33. [41c] H. B. Bürgi, *Acc. Chem. Res.* **1983**, *16*, 153−161. [41d] H. B. Bürgi, *Acta Crist, Sect. B.* **1988**, *44*, 445−448. [41e] S. Beyreuther, J. Hunger, G. Huttner, S. Mann, L. Zsolnai, *Chem. Ber.* **1996**, *129*, 745−757. [41f] S. Beyreuther, A. Frick, J. Hunger, G. Huttner, B. Antelmann, P. Schober, R. Soltek, *Eur. J. Inorg. Chem.* **2000**, 597−615.

[42] The program package YAMMP is available from: http://uracil.cmc.uab.edu/YammpWeb/

[43] D. Heisterberg, **1990**, unpublished results; the program is available from the software archive of the Computational Chemistry List (CCL) at http://ccl.ose.edu/chemistry.html

[44] D. Levine, Argonne National Laboratory, **1995**; the package is available at http://www.mcs.anl.gov/pgapack.html

[45] W. Gropp, E. Lusk, Argonne National Labratory, **1996** (available from http://www.mcs.anl.gov/mpi).

[46] *SigmaPlot for Windows Version 4.01*, Copyright 1986−1997, SPSS Inc.

[47] J. Zupan, J. Gasteiger, *J. Neural Networks in Chemistry*, VCH Weinheim, **1993**. The program kmap version 3.0 was kindly provided by J. Gasteiger, Erlangen.

Received Novemer 12, 2001
(publication delayed on the authors' request)
[I01451]